

Enhancing surface plasmon resonances of metallic nanoparticles by diatom biosilica

Fanghui Ren,^{1,3} Jeremy Campbell,^{2,3} Xiangyu Wang,¹ Gregory L. Rorrer,² and Alan X. Wang^{1,*}

¹School of Electrical Engineering and Computer Science, Oregon State University, Corvallis, OR, 97331, USA

²School of Chemical, Biological & Environmental Engineering, Oregon State University, Corvallis, OR, 97331, USA

³These authors contribute equally to the paper

*wang@eecs.oregonstate.edu

Abstract: Diatoms are single-celled algae that make photonic-crystal-like silica shells or frustules with hierarchical micro- & nano-scale features consisting of two-dimensional periodic pores. This article reports the use of diatom frustules as an integration platform to enhance localized surface plasmon resonances of self-assembled silver nanoparticles (NPs) on the surface of diatom frustules. Theoretical and experimental results show enhanced localized surface plasmons due to the coupling with the guided-mode resonances of the frustules. We observed $2 \times$ stronger optical extinction and over $4 \times$ higher sensitivity of surface-enhanced Raman scattering of Rhodmine 6G from the NPs-on-diatom than the NPs-on-glass structure.

©2013 Optical Society of America

OCIS codes: (280.4788) Optical sensing and sensors; (160.1435) Biomaterials; (240.6680) Surface plasmons; (350.4238) Nanophotonics and photonic crystals.

References and links

1. R. Gordon, D. Losic, M. A. Tiffany, S. S. Nagy, and F. A. Sterrenburg, "The Glass Menagerie: diatoms for novel applications in nanotechnology," *Trends Biotechnol.* **27**(2), 116–127 (2009).
2. C. Jeffeyes, J. Campbell, H. Li, J. Jiao, and G. L. Rorrer, "The potential of diatom nanobiotechnology for applications in solar cells, batteries, and electroluminescent devices," *Energy Environ. Sci.* **4**(10), 3930–3941 (2011).
3. M. K. Song, S. Park, F. M. Alamgir, J. Cho, and M. Liu, "Nanostructured electrodes for lithium-ion and lithium-air batteries: the latest developments, challenges, and perspectives," *Mater. Sci. Eng.* **72**(11), 203–252 (2011).
4. D. K. Gale, T. Gutu, J. Jiao, C. H. Chang, and G. L. Rorrer, "Photoluminescence detection of biomolecules by antibody-functionalized diatom biosilica," *Adv. Funct. Mater.* **19**(6), 926–933 (2009).
5. Y. Zhang, G. Liu, and H. Li, "Development of a micro-swimming robot using optimized giant magnetostrictive thin films," *Appl. Bionics Biomech.* **3**(3), 161–170 (2006).
6. C. Jeffryes, R. Solanki, Y. Rangineni, W. Wang, C. H. Chang, and G. L. Rorrer, "Electro-luminescence and photoluminescence from nanostructured diatom frustules containing metabolically inserted Germanium," *Adv. Mater.* **20**(13), 2633–2637 (2008).
7. D. Losic, J. G. Mitchell, R. Lal, and N. H. Voelcker, "Rapid fabrication of micro- and nanoscale patterns by replica molding from diatom biosilica," *Adv. Funct. Mater.* **17**(14), 2439–2446 (2007).
8. D. Losic, G. Rosengarten, J. G. Mitchell, and N. H. Voelcker, "Pore architecture of diatom frustules: potential nanostructured membranes for molecular and particle separations," *J. Nanosci. Nanotechnol.* **6**(4), 982–989 (2006).
9. Y. Yu, J. Addai-Mensah, and D. Losic, "Synthesis of self-supporting gold microstructures with three-dimensional morphologies by direct replication of diatom templates," *Langmuir* **26**(17), 14068–14072 (2010).
10. Y. Fang, V. W. Chen, Y. Cai, J. D. Berrigan, S. R. Marder, J. W. Perry, and K. H. Sandhage, "Biologically enabled syntheses of freestanding metallic structures possessing subwavelength pore arrays for extraordinary (surface plasmon-mediated) infrared transmission," *Adv. Funct. Mater.* **22**(12), 2550–2559 (2012).
11. J. N. Anker, W. P. Hall, O. Lyandres, N. C. Shah, J. Zhao, and R. P. Van Duyne, "Biosensing with plasmonic nanosensors," *Nat. Mater.* **7**(6), 442–453 (2008).
12. M.-G. Kang, T. Xu, H. J. Park, X. Luo, and L. J. Guo, "Efficiency enhancement of organic solar cells using transparent plasmonic Ag nanowire electrodes," *Adv. Mater.* **22**(39), 4378–4383 (2010).
13. J. Sabarinathan, J. Topol'ancik, S. Chakravarty, P.-C. Yu, and W. Zhou, "Quantum dot photonic crystal light sources," *Proc. IEEE* **93**(10), 1825–1838 (2005).
14. S. S. Acimović, M. P. Kreuzer, M. U. González, and R. Quidant, "Plasmon near-field coupling in metal dimers as a step toward single-molecule sensing," *ACS Nano* **3**(5), 1231–1237 (2009).
15. P. C. Lee and D. J. Meisel, "Adsorption and surface-enhanced Raman of dyes on silver and gold sols," *Phys.*

- Chem. **86**(17), 3391–3395 (1982).
16. S. Liu, T. Zhu, R. Hua, and Z. Liu, “Evaporation-induced self-assembly of gold nanoparticles into a highly organized two-dimensional array,” *Phys. Chem. Chem. Phys.* **4**(24), 6059–6062 (2002).
 17. M. Qi, E. Lidorikis, P. T. Rakich, S. G. Johnson, J. D. Joannopoulos, E. P. Ippen, and H. I. Smith, “A three-dimensional optical photonic crystal with designed point defects,” *Nature* **429**(6991), 538–542 (2004).
 18. S. Panigrahi, S. Prahara, S. Basu, S. K. Ghosh, S. Jana, S. Pande, T. Vo-Dinh, H. Jiang, and T. Pal, “Self-assembly of silver nanoparticles: synthesis, stabilization, optical properties, and application in surface-enhanced Raman scattering,” *J. Phys. Chem. B* **110**(27), 13436–13444 (2006).
 19. M. Hu, J. Chen, Z.-Y. Li, L. Au, G. V. Hartland, X. Li, M. Marquez, and Y. Xia, “Gold nanostructures: engineering their plasmonic properties for biomedical applications,” *Chem. Soc. Rev.* **35**(11), 1084–1094 (2006).
-

1. Introduction

Diatoms are a group of single-celled photosynthetic algae that make skeletal shells of hydrated amorphous silica, called frustules, which possess nanoscale patterning reminiscent of photonic crystals. Diatom frustules are produced by a bottom-up approach at ambient temperature and pressure [1], providing a cost-effective and scalable source of photonic crystal structures. These low cost, biological nanophotonic structures display versatile morphologies and may have potential applications in solar cells [2], photoluminescence-based biosensors [3], drug delivery systems [4], electroluminescent/photoluminescent devices [5], and selective membranes [6]. Diatom frustules have been used as templates for fabricating complex, spatially-patterned, metallic nano-structures including the deposition of gold (Au) and silver (Ag) coatings onto diatom frustules via self-supported gold microstructures with complex three-dimensional (3-D) morphologies using electrodeless deposition [7,8]. Theoretical analysis and experimental investigation of surface plasmons on diatom frustules are rare. Extraordinary optical transmission (EOT) at mid-infrared wavelengths (3~5 μm) has only recently been reported on freestanding metallic structures using diatom frustules as templates [9]. Plasmonic resonances at visible wavelengths associated with the intrinsic surface plasmon frequencies of noble metals such as Ag and Au, which have tremendous engineering potential for biosensors, have not been investigated on diatom frustules [10–12].

In this paper, we theoretically and experimentally investigated the interactions between localized surface plasmons (LSPs) and guided-mode resonances (GMRs) by integrating Ag nanoparticles (NPs) onto diatom frustules. Numerical simulations indicate that the electric field (E-field) amplitude of LSPs can be significantly enhanced due to the coupling of the LSPs with the photonic structure of the diatom, especially when the Ag NPs are placed inside the pores of the frustules. By coating Ag NPs onto diatom frustules using a self-assembly method, we observed a $2 \times$ stronger optical extinction from the Ag NPs on diatom frustules than the Ag NPs on the glass substrate. SERS measurement of Rhodmine 6G (R6G) shows that the NPs-on-diatom structure provides over $4 \times$ improvement in sensitivity when compared to the NPs-on-glass structure.

2. Theoretical investigation

The diatom frustules of *Pinnularia* sp. have regular arrays of sub-micron primary pores, which are lined with a thin layer of biosilica containing several nanopores with diameters below 100nm [5]. Simulations were conducted using a three-dimensional finite element method in RF module within Comsol 3.5a. Several approximations of the diatom pore structure were made to simplify the model geometry. The diatom frustule was modeled as a flat slab with a uniform thickness (120 nm). Primary pores were assumed to have little impact on LSP coupling due to the large (200 nm) edge length. Nanopores were modeled as cylindrical air holes with a commonly observed pattern consisting of a central 50 nm pore surrounded by four 80 nm cylindrical pores. A nominal lattice constant of 450nm was used in the x- and y- directions. A 10×10 array of unit cells, as shown in Fig. 1(a), was illuminated at normal incidence with a 5 μm Gaussian beam polarized in the x-direction. The refractive index of the slab was set to 1.46 for silicon dioxide.

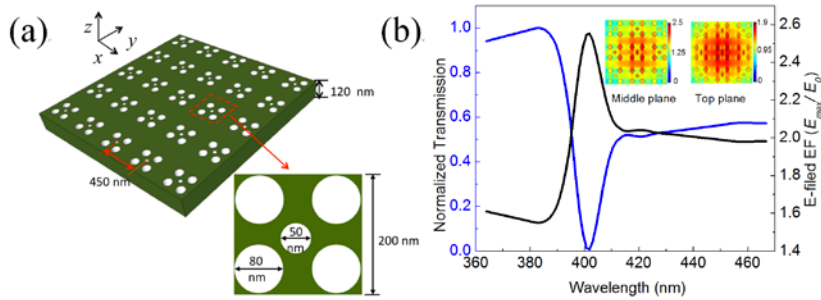


Fig. 1. (a) Diatom frustule model with 2-D periodic unit cells. (b) Simulated normalized optical transmission (blue line) and E-field EF of the diatom frustule (black line).

Due to the coupling between the discrete guided modes of the photonic crystal slab and the radiation continuum above the light line, the bio-inspired photonic structure is expected to demonstrate GMR effects with high-Q resonance [13]. The model exhibits a sharp resonance, which possesses a typical asymmetric shape around 10 nm wide at approximately 400 nm, as shown in Fig. 1(b). The E-field enhancement factor (EF) of the frustule, which is defined as the maximum E-field amplitude inside the frustule normalized to the peak E-field amplitude of the incident Gaussian beam, is also plotted in Fig. 1(b). The inset figure shows E-field amplitude distribution in the middle plane and at the top surface of the diatom frustule with peak E-field EF of $2.5 \times$ and $1.87 \times$, respectively. The maximum E-field EF is located at the middle plane of the photonic slab however E-field enhancement is still predicted at the slab surfaces.

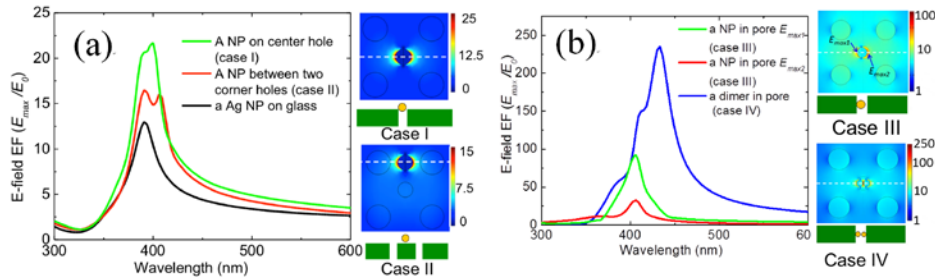


Fig. 2. (a) E-field EF of a single Ag NP on top of the diatom frustule (case I and case II) in the weakly coupled configuration (b) E-field EF of Ag NPs inside the pore (case III and case IV) in the strong coupled configuration. In (a) and (b), E-field distributions from the top view are plotted together with the schematics of the cross-section of structures.

To explore the interactions between the GMR effect of diatom frustules and LSPs of Ag NPs, we consider two different configurations. In the first configuration, the Ag NPs are coated on top of the diatom frustule. Because the GMR and the LSPs are spatially separated, we call it a “weakly” coupled configuration. Figure 2(a) shows the comparison of the maximum E-field EF of a 50nm Ag sphere NP on top of a glass substrate, the center air hole of the diatom frustule (case I), and frustule slab between the corner holes (case II). The schematics of the cross-section of structures are shown in the right panel of Fig. 2(a) together with the E-field distribution. The simulated curve in Fig. 2(a) exhibits a strong E-field EF when the Ag NP is placed on top of the central air hole (case I), which is roughly improved by $1.8 \times$ compared with the same Ag NP on a glass substrate. As a result, the total E-field enhancement of a weakly coupled system approximately equals to the product of EF from the nanoparticle and the photonic crystal structure. Compared with the E-field EFs of case I ($22.1 \times$), a weaker enhancement of case II ($16.9 \times$) is observed due to the less effective coupling of LSP mode and GMR mode. We also observed that there are two distinct peaks in the

resonant spectra of the Ag NP on the diatom frustule, where the first peak is the LSP of the Ag NP and the second is the GMR of the diatom frustule. These two resonant peaks are quite close to each other and can be barely identified.

In the second configuration, the Ag NPs are placed inside the pores to achieve a strong overlap between the GMR and LSPs, which is represented as a “strong” configuration. Such configuration is experimentally feasible if the Ag NPs are smaller than the pores. For example, Fig. 2(b) shows the simulated E-field EF of a 40 nm Ag NP that is attached to the wall of the central pore (case III). The field profile of a single NP inside the pore at the middle panel becomes highly asymmetric as shown at the upper right of Fig. 2(b). The peak E-field EF from the NP surface touching the wall (E_{max1}) is around $4.4 \times$ larger than the E-field EF in case I, which is partially due to the higher dielectric constant of the surrounding material. Nevertheless, the peak E-field EF on the other side (E_{max2}) is still larger than the maximum EF observed in Case I of Fig. 2(a). Due to the increase of effective dielectric constant, a redshifts of resonant wavelengths were observed when comparing with case I and case II. We proceed to conduct a further study on the NP dimer, which has been demonstrated that the biomedical detection sensitivity to be increased by several times compared to isolated metal NPs due to the strong field confinement [14]. A NP dimer is constructed inside the pore (case IV) as shown at the bottom right of Fig. 2(b). The model consists of two NPs with 24-nm diameter and a gap size of 2 nm, which results in a maximum EF inside the pore as high as $235 \times$. For a NP dimer, the resonant wavelength further redshifts to 433 nm, which is attributed to the enhancement of the particle near-field coupling.

3. Experimental results

Diatoms were cultured in 500mL flasks containing 100mL of Harrison’s artificial seawater medium with a seeded cell density of 5×10^4 cells•mL⁻¹ and an initial silicic acid concentration of 0.5 mM. Cultures were incubated for 72 hrs at 22°C, illuminated at $30 \mu\text{M m}^{-2} \text{sec}^{-1}$ on a 14:10 light: dark cycle. Glass substrates (22mm \times 22mm) were placed in 60 mm petri dishes and covered with 15 mL of the diatom cell suspension. Cells were allowed to settle onto the substrates for 45-60 minutes under $150 \mu\text{M m}^{-2} \text{sec}^{-1}$ illumination. Liquid was collected and substrates were transferred to clean 60 mm petri dishes, sealed with Parafilm and maintained under illumination for 48 hours at ambient relative humidity (RH < 30%). Residual cells were collected from seeding dishes and combined with collected liquid media for analysis of residual cell counts. Following incubation, biofilms were soaked for four hours in 70% ethanol and four hours in 100% ethanol to stabilize the films and remove soluble organic materials. Biofilms were dried in air and UV-O₃ cleaned for 12 hours at 90°C with filtered air supplied at 0.5 scfh. The diatom frustules were annealed at 400 °C in air for 1 hour in order to improve adhesion to the glass substrate. Scanning electron microscopy (SEM) image of a representative diatom is presented in Fig. 3(a). Ag nanoparticles solution was prepared by the Lee and Mesel Method, which can be found in reference [15]. The diatom-coated substrates were modified with aminopropyltriethoxyl-silane (APTES) to promote NP adhesion, where the method is described in reference [16]. To start with this process, the glass substrate that coated with diatoms was first cleaned by immersing in a solution (1:1:5H₂O₂/NH₄OH/H₂O) for 1 h at 70 °C, followed by rinsing with deionized water and rinsing in methanol. High-density hydroxyl groups on glass substrate and diatom surface were created due to this pretreatment, which were used to attach the APTES molecules. After cleaning, the diatom samples were immersed in APTES (10%, by weight in methanol) solution for 5 hours, followed by rinsing successively in methanol and deionized water and blowing with high-purity nitrogen. The substrates were then exposed to an Ag colloidal suspension for 12 h to deposit the Ag NPs onto the frustules and the underlying substrate. After being removed from the NP solution, the sample was rinsed with deionized water and dried with high-purity nitrogen. The representative SEM image in Fig. 3(b) shows the densely assembled Ag NPs on the diatom frustule. Various nanoparticle morphologies are formed, including isolated NPs, NP dimers, trimers, short chains and nanorods on top of the frustule and the glass substrate, which give multiple plasmonic resonances depending on the

aggregation states of the Ag NPs. The average size of the NPs in our preparation is larger than the nanopores, therefore the relative number of NPs located within the diatom pores may be small. Figure 3(c) shows a dark-field image of self-assembled Ag NPs on diatom frustules demonstrating strong contrast due to optical scattering compared to the self-assembled Ag NPs on the surrounding glass substrate.

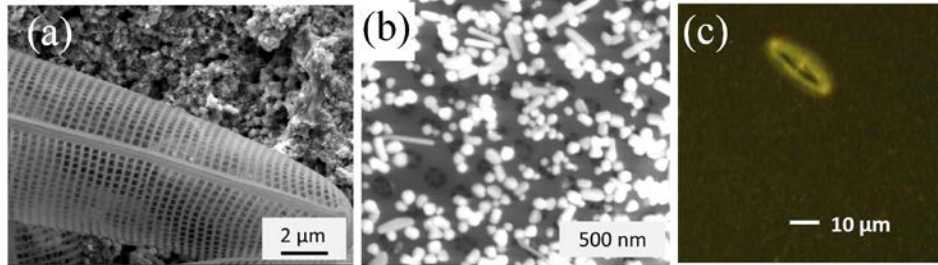


Fig. 3. SEM pictures of (a) a diatom frustule, (b) Ag NPs self-assembled on the diatom frustule; (c) Dark-field image of self-assembled Ag NPs on diatoms frustules and on glass substrates.

We measured the extinction spectra to study the interactions between the diatom frustules and the Ag NPs [17]. A broadband white light source (Intralux 6000) was used as the excitation source. The light was focused by a $40\times$ objective lens ($NA = 0.65$), which was then coupled into a lensed fiber to focus light into the diatom frustules. The sample is mounted on a three-dimensional translation stage. The transmitted light after the sample was collected by a bundled fiber and measured by an Ocean Optics USB4000 spectrometer. The extinction spectra of an unmodified diatom frustule, Ag NPs coated on a flat glass substrate, and Ag NPs coated on a diatom frustule were investigated. We observed a broad, low-Q resonance between 380 nm-720 nm with a peak extinction at around 480 nm, as shown in Fig. 4(a). The reduced Q-factor of the observed GMR is believed to be affected by different sources of imperfections including variation of the lattice periodicity, surface roughness, and curvature of the frustules which will cause angular dependence of the incident light. This broadband resonance may help to increase the overall photosynthetic efficiency for diatom over the entire spectrum of visible light.

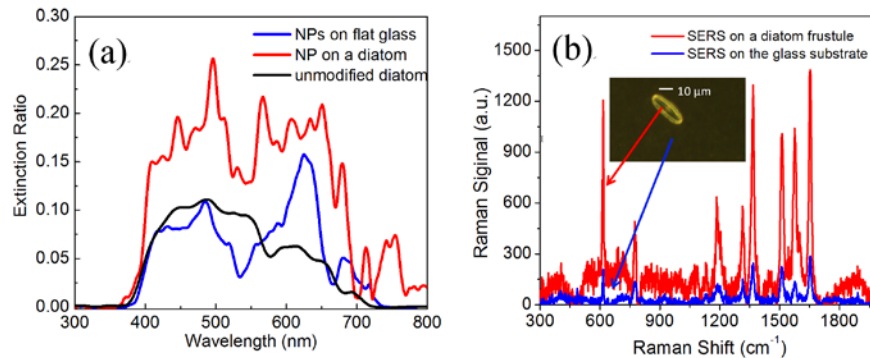


Fig. 4. (a) measured extinction spectra of unmodified diatom (black), Ag NPs on glass (blue) and NPs on a diatom frustule (red). (b) SERS spectra on a diatom frustule (red) and on the glass substrate (blue). The inset picture shows where the SERS signals are collected

The interaction of the Ag NPs with the nanostructured diatom biosilica was also studied. Previous studies have shown that the wavelengths of the LSP resonances at the metal surfaces are determined by the overall geometries and the aggregation states of the Ag NPs [18]. Compared with a single NP, the aggregation of Ag NPs induces plasmonic extinction at longer wavelengths when individual nanoparticles are in a close-packed assembly and

coupled to each other. The frequency and intensity of the plasmon oscillation depend on the degree of aggregation as well as orientation of the individual particles within the aggregate with respect to the polarization direction of the excitation light. For the Ag nanorods, the LSP splits into two modes: one transverse mode with a resonant frequency close to a single nanoparticle (low extinction amplitude), and one longitudinal mode resonant at a much longer wavelength (strong extinction amplitude), which is determined by the nanorod geometry (size and aspect ratio) [19]. In our measurement, the extinction spectrum of Ag NPs observed on the glass substrate shows only two broad resonances: the broad extinction peaks centered at 487 nm and another broad resonance observed at 630 nm. The broadening is due to the excessive radiation damping from large-size nanoparticles, as well as the overlap of multiple resonances of similar aggregation states that have close resonant frequencies. The broad extinction peaks centered at 487 nm are possibly due to the resonances of Ag NP spherical aggregates (dimers, trimers, and short chains), whereas the coupling of Ag nanorod dipoles give rise to the broad resonance observed at 630 nm. However, the extinction peaks due to individual aggregation states cannot be clearly identified due to the variations in the nanoparticle dimensions. In the presence of the diatom frustule, we observe two significant differences as shown in Fig. 4(a): 1) the diatom frustule increases the optical extinction ratio of the NP aggregates relative to NPs on flat glass, which is nearly $2 \times$ stronger, on average, between 400 nm to 700 nm; 2) the Q-factors of those LSPs are enhanced by the diatom frustule so that individual LSPs become distinguishable. These differences are attributed to the coupling of the LSPs and the GMR effects of the diatom frustules.

To verify whether the enhanced LSPs on diatom biosilica can contribute to plasmonic biosensing, NPs-on-diatom substrates were used as SERS substrates for molecular detection. In the SERS measurement, R6G (20 μ L, 1 μ M in ethanol), which is widely used as SERS probing molecules, was drop-coated on the sample surface and evaporated to dryness. Samples were analyzed using a Horiba Jobin-Yvon HR800 confocal Raman spectrophotometer with a 532nm diode laser (1.4 μ m spot size), and a Synapse CCD detector. Measurements were taken using a $50 \times$ objective lens (NA = 0.75), 100 μ m confocal hole and 1 second integration time. The laser spot size was sufficiently small to be completely contained within a single frustule. The single-point SERS signals measured on the flat glass and on the diatom frustule are plotted in Fig. 4(b). The inset picture shows where the Raman signals were collected for these two measurements. Using the major R6G Raman peaks at 614 cm^{-1} , 776 cm^{-1} , 1368 cm^{-1} , 1511 cm^{-1} and 1651 cm^{-1} , the Raman signal intensity is enhanced by a factor of 4.79 ± 0.8 , which clearly indicates enhancement of the LSPs due to the presence of the diatom frustule.

4. Summary

In conclusion, we have investigated LSPs on diatom biosilica by integrating different Ag NPs and NP clusters into the frustules. Simulation of such interactions predicts stronger optical extinction and enhanced localized electric field compared with NPs on a flat glass substrate, which is attributed to the coupling between GMRs and LSPs. By focusing white light onto an individual diatom frustule, our experimental measurements of the extinction spectra confirm the coupling of the two optical resonances. The potential of such Ag NPs-on-diatom nanophotonic structure has been confirmed by the SERS measurements of R6G with over $4 \times$ improvement in sensitivity compared to Ag NPs on glass. The enhanced LSPs on diatom biosilica may find widespread use in plasmonic sensing.

Acknowledgment

G.L. Rorrer acknowledges support of this research by the National Science Foundation (NSF) through the Emerging Frontiers in Research and Innovation (EFRI) program, award number 1240488. A. X. Wang acknowledges support by the School of Electrical Engineering and Computer Science at Oregon State University. The authors would like to thank Materials Synthesis and Characterization Facility (MASC), and Dr. Thomas K. Plant for the support in nanoparticle preparation and optical characterization.